PERGAMON

International Journal of Heat and Mass Transfer 45 (2002) 4141–4150

International Journal of HEAT and MASS TRANSFER

www.elsevier.com/locate/ijhmt

Fringe probing of an evaporating microdroplet on a hot surface

Wangcun Jia [a], Huihe Qiu [b,*]

[a] Department of Mechanical and Aerospace Engineering, University of California, Los Angeles, CA 90095, USA

[b] Department of Mechanical Engineering, Hong Kong University of Science and Technology, Clear Water Bay, Kowloon, Hong Kong

Received 19 November 2001; received in revised form 14 March 2002

Abstract

The phenomenon of droplets impacting and evaporating on a hot surface is of interest in many areas of engineering. Quantitative measurement of these processes provides great help to reveal the physics behind. A novel technique was developed to quantitatively measure the volume evolution and contact diameter of an evaporating microdroplet on a hot surface utilizing interference fringe scattering method. In this method, fine fringes produced by the interference of two coherent laser beams was scattered by the droplet and projected onto a screen. The profile and volume of the droplet can be derived from the spatial fringe spacing on the screen. The number of total fringes measurable on the screen was used to determine the instantaneous contact diameter of the microdroplet. Validation experiments demonstrated that the measurement errors are less than $\pm 5\%$ and $\pm 1\%$ for microdroplet volume and contact diameter, respectively. By using this method, the dynamic of droplet impingement, evaporation and boiling using ethanol, pure water and water solution of a surfactant (sodium dodecyl sulfate) with impact velocity of 7.5 m/s and diameters ranged from 0.19 to 0.46 mm were investigated.

Keywords: Droplet evaporation; Optical profile measurement; Spray cooling

1. Introduction

Knowledge of the impacting and evaporating behavior of individual droplets on a hot solid surface is not only essential for the prediction of droplet impact cooling, but also of interest in many areas of engineering such as the study of combustion engines and fire safety situations. In these applications, the dynamic behavior of the impinging droplet and the heat and mass transfer between a droplet and a hot surface are important phenomena. A fundamental understanding of these phenomena requires the ability to record the progressive stages of deformation and evaporation of the droplet. Various techniques have been developed to this end. High-speed cine film and short duration single shot photography were often used in previous research. These include the photographic studies of Wachters and Westerling [1], Toda [2], Chandra and Avedisian [3], Xiong and Yuen [4] and Qiao and Chandra [5]. Xiong and Yuen [4] investigated the evaporation of liquid droplets ranging from 0.07 to 1.8 mm with relatively low velocity of 0.4 m/s, including water and various pure and mixed hydrocarbon fuels on a hot stainless steel plate. A strobe-video visual system is used to record the evaporation process. Qiao and Chandra [5] studied droplet boiling on a hot stainless steel surface using both video and 35 mm cameras. Water and water solution of a surfactant were used as test liquid. Droplets were dropped from a hypodermic needle at 50 mm above the test surface with a diameter of about 2 mm. They concluded that heat transfer could be enhanced by adding surfactant because surfactant reduces contact angle of droplets and promotes nucleation of vapor bubbles and cause foaming.

* Corresponding author. Tel.: +852-2358-7190; fax: +852-2358-1543.

E-mail address: meqiu@ust.hk (H. Qiu).

0017-9310/02/$ - see front matter
PII: S0017-9310(02)00131-X

Nomenclature

c	geometry constant
d	impinging droplet diameter
D	contact diameter
h	interference fringe spacing
k	liquid refractive index dependent constant
L	distance between droplet and screen
m	relative refractive index
n	total scattering fringes number
r	radial displacement from center of droplet
R	radius of droplet
V	droplet impinging velocity
x, y	Cartesian coordinate
y, y', y''	local height of droplet, first-, second-order derivative

Greek symbols

α	angle
λ	wavelength
θ	contact angle

Subscripts

e	end
i	incident
r	refraction
s	scattering, start

Laser interferometric techniques, which normally provide higher accuracy than the photography techniques, have been developed to measure the profiles of a transparent object. However, previous optical methods focused on the profiles of large objects, such as the diameter of objects larger than several millimeters [6–8]. Xu et al. [9] developed a method, based on holographic and shearing interferometry, to measure the profile of liquid droplets on flat, horizontal glass substrates. Although this method is simple in principle, great effort and high precision in setting up are necessary. Furthermore, it is too difficult to heat the substrate by using this method. In the reflection-interference method developed by Guo et al. [10], the interference fringes must be measured at a location that depends on the droplet's shape. Because an evaporating droplet may change its shape, it is not feasible to implement this method. The technique based on intensity developed by Thomas et al. [11] is inaccurate in practice since the scattering intensity is sensitive to the distortion of background scattering and wall reflection. In summary, a feasible optical method that is capable of measuring the profile and volume of a deformed droplet during evaporation is necessary.

In this research, the evaporation of a microdroplet on a hot surface is visualized and measured by an improved optical method [12]. In this method, very fine parallel fringes produced by a Mach–Zehnder interferometer are projected onto the base of a droplet. The fringes scattered by the deformed droplet are enlarged and formed on a screen. Through geometrical optics approach, the profile of a droplet can be derived from the spatial frequency of the scattering pattern on the screen. By assuming the droplet is rotationally symmetric about its vertical centerline, the volume of the droplet is obtained from its profile. Finally, the evaporation process is analyzed by processing the recorded series of the scattering pattern.

2. Geometrical optics approach

The schematic diagram of the optical system is shown in Fig. 1 where a microdroplet was located at the top surface of a quartz cylinder and illuminated by parallel interference fringes produced by a Mach–Zehnder interferometer. The scattering rays from the microdroplet were projected onto a screen where the deformed fringe pattern was recorded by a CCD camera. The reflection from the interfacial surface between the microdroplet and the substrate was negligible because of little difference in the refractive index between quartz and working liquid.

By using geometrical optics approach and assuming the microdroplet is a segment of a sphere as shown in Fig. 2 (In fact, this assumption is not necessary as indicated later.), the following equation can be derived [12]:

$$\frac{r}{R} = \frac{\sin\alpha_s}{(1 - 2m\cos\alpha_s + m^2)^{1/2}} \tag{1}$$

where r, R, α_s are shown in Fig. 2 and m is the relative refractive index of liquid.

If r/R is less than 0.58, a linear function of α_s with a maximum error of $\pm 10\%$ can be expected. If r/R is greater than 0.58, or the contact angle is higher than 35°, an extension of this method is also proposed [13]. For a water droplet on a glass substrate, the maximum r/R is 0.24 [14]. Thus, the non-linear error drops to less than 1% and Eq. (1) leads to:

$$\frac{r}{R} = k\alpha_s \quad \text{or} \quad \frac{\Delta r}{R} = k\,\Delta\alpha_s \tag{2}$$

where k is a constant, which depends on the liquid refractive index, and $\Delta r = h$ is the fringe distance.

Considering two fringes and noticing that $L \gg \Delta x$ and $\Delta x \gg h$ (see Fig. 3), the relation between Δx and $\Delta\alpha_s$ can be written as:

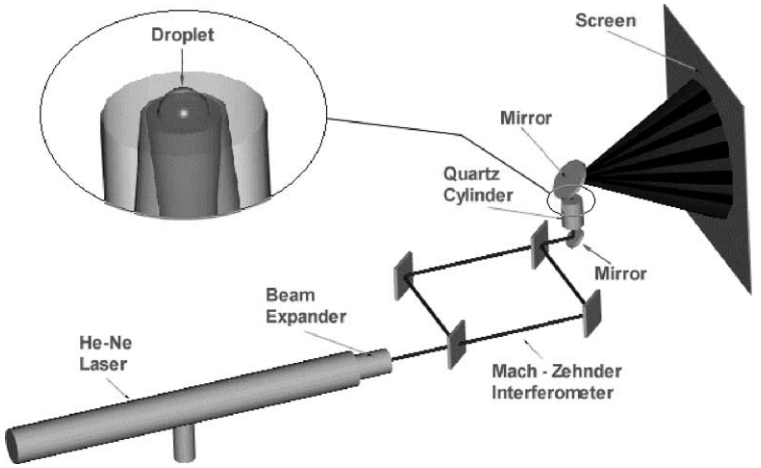

Fig. 1. Optical set-up of experimental facility.

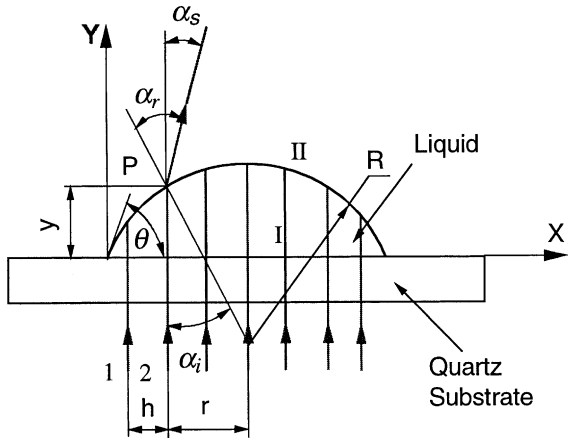

Fig. 2. Scattering angle definition.

$$\Delta\alpha_s \approx \frac{\Delta x}{L} \tag{3}$$

where Δx is the projected fringe spacing and L is the distance between the microdroplet and the screen. Substituting Eq. (3) into Eq. (2), the radius of the microdroplet can be calculated as:

$$R = \frac{hL}{k\Delta x} = c\frac{1}{\Delta x}; \quad c = \frac{hL}{k} \tag{4}$$

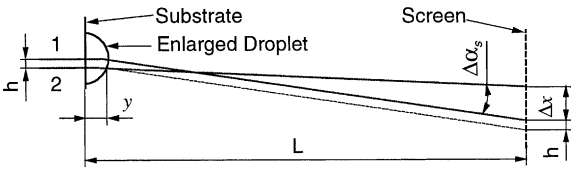

Fig. 3. Relation between $\Delta\alpha_s$ and Δx.

where the constant c is determined by the optical configuration. This is the equation for calculating the radius of a spherical-cap-shaped droplet on a transparent substrate. It is shown that the fringe spacing on the screen is inversely proportional to the radius of the spherical-cap-shaped droplet. Because the spacing of incident fringes is uniform, i.e. h is a constant, and the radius of the curvature remains unchanged along the whole spherical segment, the scattering fringes on the screen have a uniform spacing. Therefore, the average fringe spacing, $\overline{\Delta x}$, can be used to calculate the radius R.

Eq. (4) can also be extended to measure the local curvature of a non-spherical droplet, which is commonly encountered in practice. If the droplet is a non-spherical segment, it is expected that the spacing of the scattering fringes on the screen vary accordingly. Let us consider a non-spherical droplet shown in Fig. 4. Fringes 1 and 2 intersect the droplet at points P_1 and P_2, respectively. If the difference between the local radius of curvatures R_1 and R_2 is negligible, i.e. $R_1 \approx R_2 \approx R$, Eq. (4) is still valid under this assumption. This assumption is reasonable

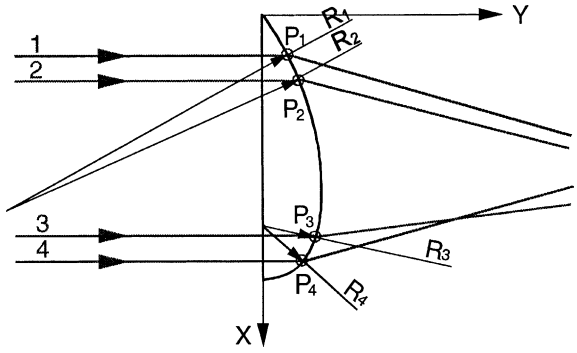

Fig. 4. Non-spherical droplet.

because the droplet curvature changes smoothly in practice and segment P_1–P_2 is very small since the incident fringe spacing is one order of magnitude smaller than the droplet contact diameter. Similarly, $R_3 \approx R_4 \approx R'$ can also make the validity of Eq. (4). Hence, the local radius of curvature of the whole droplet can be derived from the spatial frequency of the scattering fringes on screen.

Droplet profile $y(x)$ can be reconstructed from the measured curvatures. The differential equation governing the relationship between the local radius of curvature $R(x)$ and the local height $y(x)$ is:

$$R(x)|y''| - \left(1 + y'^2\right)^{2/3} = 0 \tag{5}$$

The radius of curvature $R(x)$ is obtained through interpolation of experimental data.

Eq. (5) can be solved numerically if the boundary conditions, $y(0)$ and $y'(0)$, are known. Without losing generality, the starting point of the droplet profile can be surmised as $x_s = 0$ and $y_s = 0$. To determine $y'(0)$, let us consider a typical scattering pattern of a droplet as shown in Fig. 5. In addition to the fringe spacing, the total fringe number, n, is another important parameter, which means the droplet covers n fringes. Therefore, the span of the droplet is:

$$x_e = nh \tag{6}$$

Because the ending point of the profile is coplanar with the start point, we have the following boundary conditions as a supplement:

$$\begin{cases} x_s = 0, & y_s = 0 \\ x_e = nh, & y_e = 0 \end{cases} \tag{7}$$

Eq. (5) can be solved by fourth-order Runge-Kutta method with giving an initial value $y'(0)$. The calculated y_e may not be zero, so the initial $y'(0)$ is iterated in the numerical calculation until the above boundary conditions are fulfilled. The volume of the droplet can be calculated by integrating the revolved solid along the centerline of the profile.

3. Experimental apparatus and calibration

The schematic diagram of the experimental apparatus is illustrated in Fig. 1. It consists of a Mach–Zehnder interferometer, a quartz cylinder with its heating, temperature controlling system and a CCD camera behind the screen. A microdroplet was placed on the substrate where the fringe pattern of the incident beam was generated by the two-beam interference. A 15 mW He–Ne laser was used as the light source. The screen was located at 324 mm from the substrate and the images on the screen were recorded by a Sony digital video camera TRV-900E. The detailed parameters of the test facility and conditions are shown in Table 1.

Based on current parameters, the accuracy of the method is analyzed. The measured contact diameter is discrete and the step is the spacing of the interference fringes e.g., 45 μm. If there are total n fringes, the average measurement error is $1 - (n/(n + 0.5))$. If $n = 5$, the average possible error is 9%. The accuracy can be improved by using fine fringes, which can be produced by the laser of short wavelength. The measurable minimum volume is determined with the minimum contact diameter and maximum measurable radius of curvature. The minimum contact diameter is 225 μm if $n = 5$ for an acceptable accuracy. The maximum measurable radius is limited by the possible minimum spacing of the fringes on the screen. Because there is a beam stop of 14×8 mm to attenuate the high intensity incident beams (see Fig. 5), the minimum area of scattering pattern should be as twice as the area of the stop in order to remove the image of the stop by interpolating the fringes surrounding it. Thus the minimum spacing of

Table 1
Parameters and conditions

λ (μm)	L (mm)	m	c	h (μm)	$T_{ambient}$ (°C)	RH
0.6328	324.0	1.34	2.50	45	20	60%

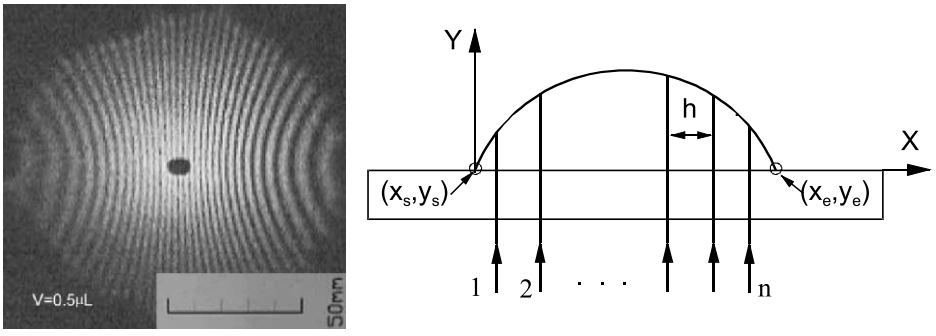

Fig. 5. A typical scattering pattern of a droplet.

the fringes on the screen is 14 mm/n and the maximum radius of the droplet is $R_{max} = (nhL/14k)$. If $n = 5$, $R_{max} = 2.08$ and the minimum volume is 2.48×10^{-5} mm^3, the diameter of corresponding sphere is 36 μm.

3.1. Calibration of diameter of contact circle

As indicated by Eq. (7), the span of the droplet or the diameter of the contact circle, x_e, is used as a boundary condition to reconstruct the droplet profile and to calculate the volume and x_e is derive from Eq. (6). The assumption to use Eq. (6) to calculate x_e is that the edge of the droplet is located just at the centers of two bright fringes. However, the edge of a droplet is located randomly on the substrate during impingement and evaporation. Furthermore, most liquids, particularly those with high wettability, have very gradual changes in their profiles near the solid–liquid contact line. This causes difficulty in experiments in clearly observing or accurately measuring the contact edge. Therefore, calibration experiments to improve Eq. (6) are necessary.

In the calibration experiments, the droplet image under a microscope and the corresponding scattering fringe pattern were recorded almost simultaneously. The detailed experimental set-up can be found in Jia [13]. The recorded image and fringes of a droplet are shown in Fig. 6. The contact diameter of the droplet measured from the image is assumed to be the actual diameter. Comparisons of the actual and calculated diameters by Eq. (6) are shown in Table 2, where n is the total number of fringes. It is found that the calculated diameters are smaller than the actual diameters. This is because the edge of the droplet was not located exactly on the bright fringe. If the total number of fringes is compensated by two, one for each side, the difference between the calculated and actual diameters is acceptable. Accordingly, a compensated total fringe number is used in the profile reconstruction and volume calculation. The radius of the new segment was obtained by using the extrapolation method.

3.2. Calibration of volume measurement

The volume measurement was calibrated by measuring a water droplet with known volume on the substrate. Tiny water droplets were delivered onto the substrate by means of a 0.5 mm^3 capacity Hamilton microsyringe. Because the surface tension of water is high, a spherical water droplet on the needle's tip can be transferred to the substrate entirely. The syringe was thus used to measure the nominal volume of droplets. Since the CCD camera was turned on before a droplet was put onto the substrate, a series of fringe patterns were recorded. Because a water droplet evaporates slowly at room temperature, it is reasonable to calibrate the method with the volume calculated from the first frame after the initial deformation. The calibration result is shown in Fig. 7. It is found that the discrepancy between the measured volume and nominal value is ±5%. This method is thus adequate in engineering applications. The remaining error may be caused by asymmetry of the droplet.

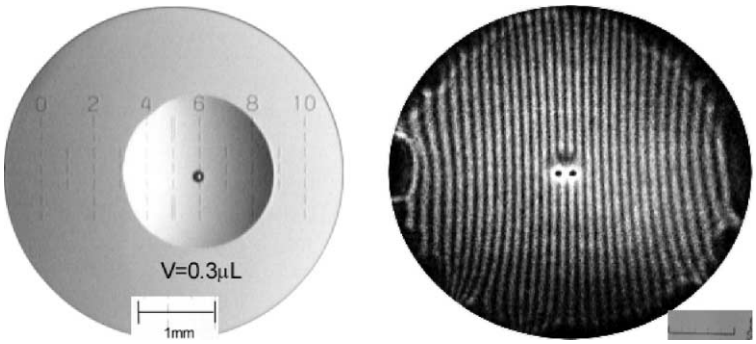

Fig. 6. Image and fringes for same droplet with volume = 0.3 mm^3.

Table 2
Comparisons of actual and calculated diameters

Volume (mm^3)	D by image (mm)	h (mm)	$x_e = hn$ (mm)	Error (%)	$x_e = h(n+2)$ (mm)	Error (%)
0.3	1.845	0.114	1.596	−13.5	1.824	−1.1
0.3	1.721	0.049	1.590	−7.6	1.689	−1.8
0.5	2.142	0.049	2.037	−4.9	2.136	−0.2
0.5	1.965	0.049	1.888	−3.9	1.987	1.14

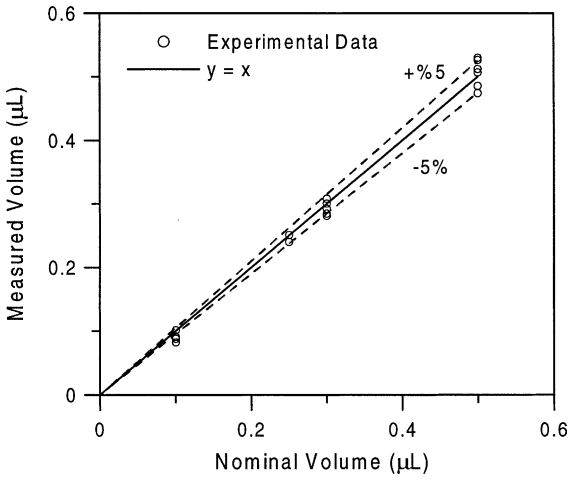

Fig. 7. Relation between calculated and nominal volume.

4. Measurement of transient droplet evaporation

In most previous experimental studies, the impinging droplets were produced by a hypodermic syringe. The droplet diameters in those studies were larger than 1 mm, and the droplet velocities were around 1 m/s, in general. In spray cooling, microdroplets ($d = 30$–300 μm) impact the hot surface with high velocity ($V = 5$–10 m/s).

In the experiments, high velocity microdroplets were produced by a vibrating orifice mono-disperse droplet generator (TSI model 3450). By using a 20 μm orifice under 3.75 mm^3/s liquid feed rate and 20 kHz vibrating frequency conditions, mono-dispersed droplets with a diameter of 71 μm and a velocity of 7.5 m/s can be produced. A blocker driven by an electromagnet shaker was used to select the number of droplets impinging on the surface as shown in Fig. 8. Normally, the top edge of the blocker was located in the path of the droplet stream, thus no droplet can reach the substrate. Once a short pulse with known duration applied to the input of the electromagnet, the blocker released the stream path and the selected number of droplets can impinge onto the substrate. Because of high droplet impinging frequency and relatively low blocker reciprocating speed, it is difficult to select only one droplet impacting on the substrate. Therefore, several sequentially impinged microdroplets will coalesce to form a large droplet on the substrate. Fortunately, because the time interval of impingement and coalescence is in milliseconds range which is at least two order of magnitude shorter than the evaporation time (in several hundreds of milliseconds or larger). Therefore, the heat transfer and evaporation can be considered to take place well after the coalescence has been completed. The initial volume of the coalesced droplet can be calculated by the number of droplets arrived on the substrate during the pulse duration. It can also be measured directly by the newly proposed method as described previously. Of course, if a precise camera shutter with a short duration of 1/10,000 s (It has been commercial available.) or a low frequency droplet generator can be used, single microdroplet impingement can be obtained.

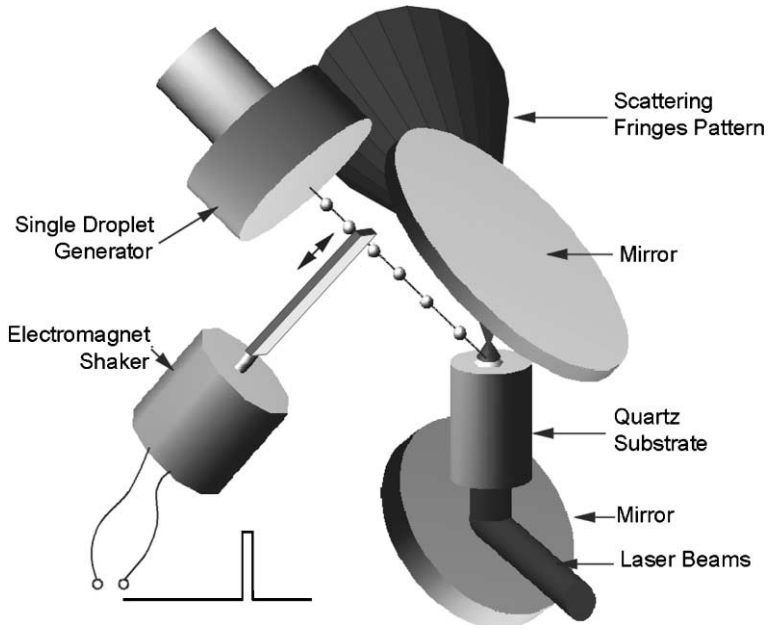

Fig. 8. Experimental set-up for droplet impingement.

Using above set-up, quantitative measurements of the transient impinging and evaporation processes for droplets of different liquids on a quartz substrate with different surface temperatures were performed. Ethanol, pure water and a water solution of a surfactant with different concentrations were used. The surfactant used is sodium dodecyl sulphate (SDS), obtained in powder form from Riedel-de Han AG. The surfactant solutions were prepared at least 1 h before the experiments to minimize the presence of dissolved gases. Before the concentration of the surfactant solution was changed, the droplet generator had been cleaned with alcohol, distilled water and compressed air.

For an ethanol droplet with an initial volume of 4.2×10^{-3} mm^3, which was resulted from 22 micro-droplets' coalescence within 1.1 ms, impacting and evaporating on the quartz substrate with a surface temperature of 70 °C, 14 frames were recorded. Fig. 9 shows some frames of the recorded fringe pattern at different times. Using the newly developed method the droplet profile, volume and contact diameter can be calculated from the fringe patterns directly. The measurement results are shown in Fig. 10. It was found that the contact diameter of the ethanol droplet on the quartz surface kept in constant for a very short period (about 1 ms) and then gradually reduced with time while the contact angle was almost remained unchanged. Fig. 9 also indicates that the shape of the contact line of an ethanol droplet is not circular in shape, which may cause some measurement error if the contact shape was assumed circular. To quantify the error, the measured initial volume was compared with the nominal initial volume that was calculated by the droplet diameter and the number of droplets impacting on the substrate during the pulse duration. In Fig. 10 the measured initial volume of the ethanol droplet is 4.2×10^{-3} mm^3 but the

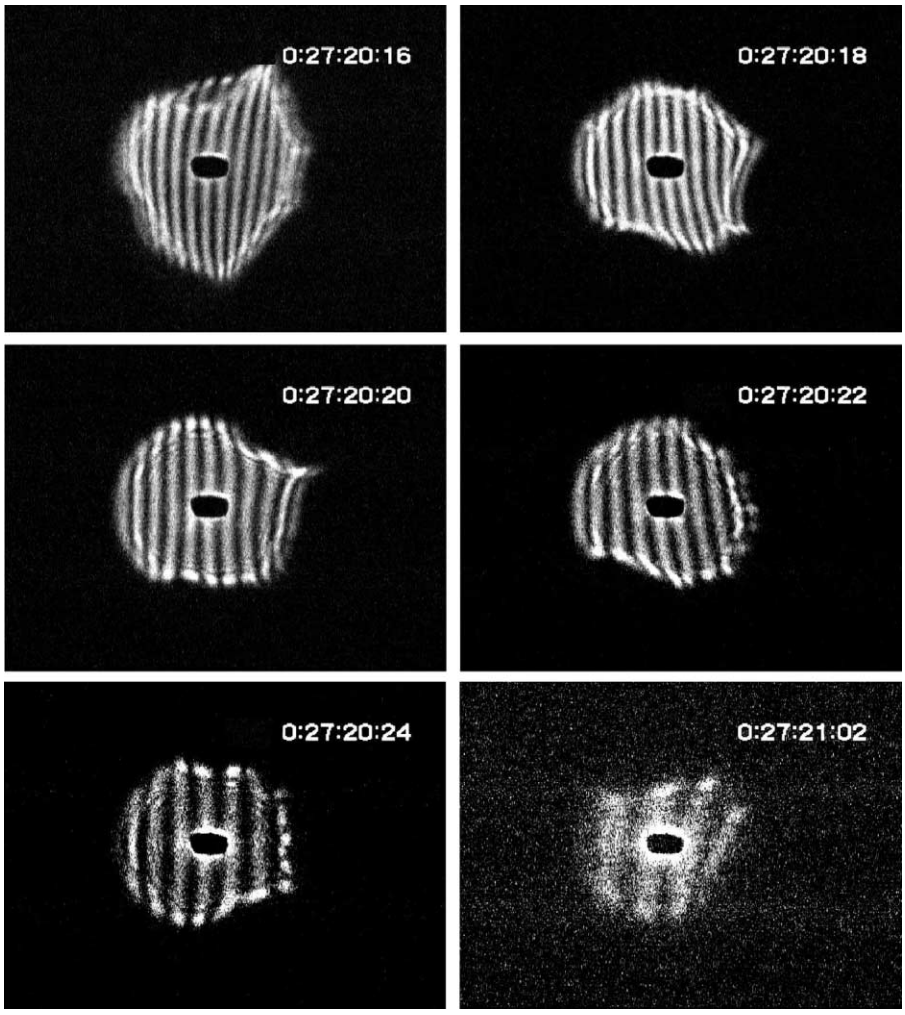

Fig. 9. Fringe pattern series of an ethanol droplet ($T = 70$ °C).

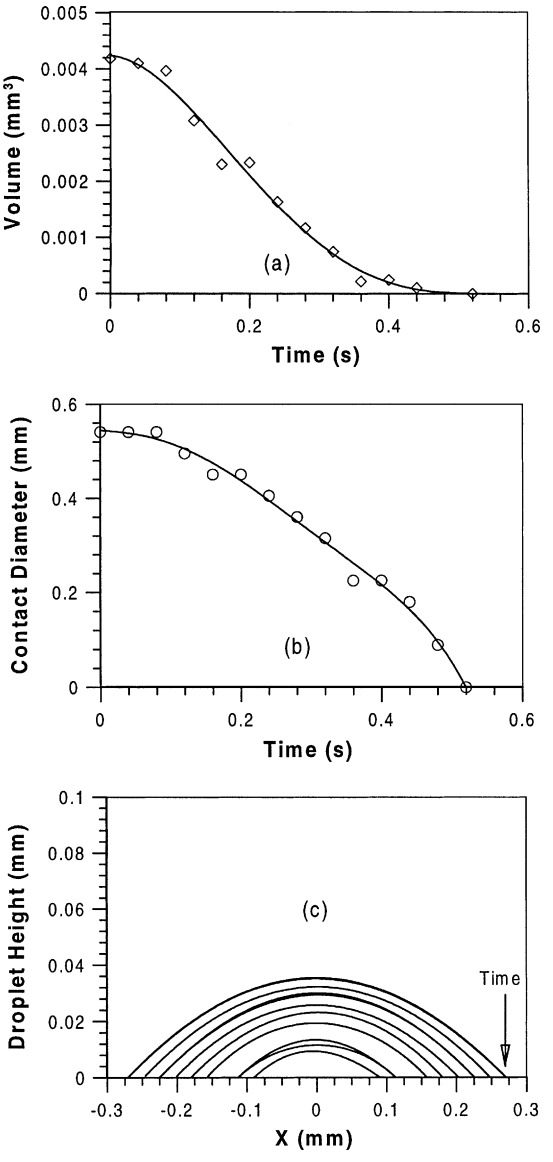

Fig. 10. Volume, diameter and profile evolution for an ethanol droplet ($T = 70$ °C).

calculated initial volume (including 22 ethanol droplets with 71 μm in diameter) is 4.12×10^{-3} mm^3, which gives a measurement error about 2%. By also considering the error in droplet diameter measurement, the total measurement error for current case lies in ±5%. It is possible to further improve the measurement accuracy with this kind of very complex shape by illuminating the droplet with two fringe generation systems. Each system is similar to the current proposed system but with different fringe direction and wavelength which will form orthogonal grid-like fringes. This fringe generating system is similar to a commonly used transmitting unit in 2-D laser Doppler anemometry.

Experiments were also conducted to investigate the effect of adding surfactant. One thousand ppm surfactant concentration was used and the droplet initial volume of 1.1×10^{-2} mm^3 was chosen. The temperature of quartz surface was 100 °C and a total of 23 frames were recorded. Fig. 11 shows the measurement contact diameter, volume and droplet profile evolution. It is found that the evaporation process can be divided into three regions as shown in Fig. 11. Region I is constant volume heating up (less than 10% change in volume) because the droplet must absorb heat to reach evaporation temperature. Region II is constant contact diameter evaporation during which the droplet contact diameter remains constant while the contact angle decreases until it reaches its minimum value. Region III is the contact diameter starting to decrease (10% less than the initial diameter). During this period the contact angle remains unchanged and, it is therefore, also called constant contact angle evaporation. This region is also very short when evaporating a water droplet. For an ethanol droplet (see Fig. 10), only regions I and III can be observed because of its high wettability.

At the end of the evaporation (region III), the thin water film shrinks. This kind of evaporation may enhance heat transfer since the ratio of the heat transfer area to the thickness increases during the evaporation process. In the modeling of dropwise evaporation, this result must also be taken into consideration as the contact angle was assumed to be constant in the past mathematical models [15,16]. Comparison between the actual profile and an arc shows that droplets were almost shaped as spherical cap during evaporation. This result is very useful to simplify the modeling of dropwise evaporation. As shown in Fig. 12, the dynamic aspect ratio is nearly constant for ethanol, but the change in the dynamic aspect ratio is very large for the case of water solution droplets.

The concentration of surfactant may increase during droplet evaporation, which may affect the refractive index of the working fluid and the liquid–solid contact angle. The refractive indices of water solution with different surfactant concentrations were measured by using a Carl Zeiss Abbe refractometer (accuracy: 0.0005). It was too difficult to identify any change in refractive index for a surfactant concentration less than 1000 ppm. Even when the concentration increases to 100,000 ppm, its refractive index changes to 1.3435, which is only 1% higher than that of pure water (1.3327). Therefore, constant refractive index of the water solution of SDS during the measurements has always been assumed. Qiao and Chandra [5] have measured the equilibrium contact angle of water and surfactant solution on a stainless steel surface. It is 90° for pure water; adding 100 and 1000 ppm of surfactant reduces the contact

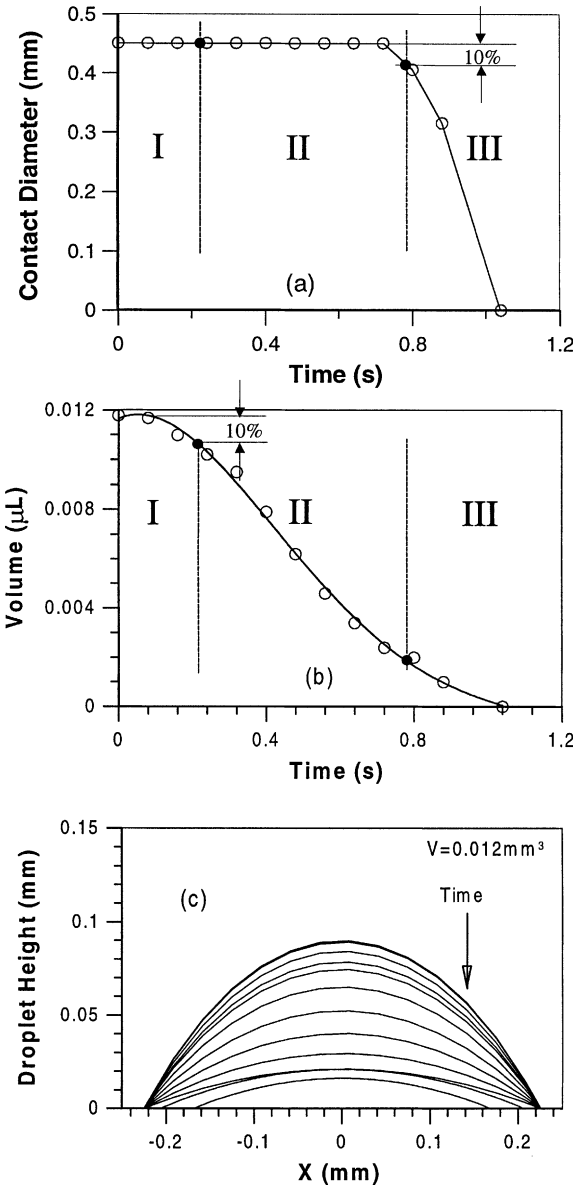

Fig. 11. Evaporating of a surfactant solution droplet (1000 ppm by weight) on a quartz surface ($V_0 = 0.012$ mm^3, $T = 100$ °C).

angle to 55° and 20°, respectively. However, the receding contact angle for water was measured to be approximately 10° and was not altered by surfactant addition. Therefore, the reduction of contact angle during evaporation (see Fig. 12) may be caused by both evaporation of water and concentration increasing of surfactant.

To evaluate the measurement capability of the new method, evaporation of droplets with different initial volumes was also studied. The initial volume was changed with adjusting the width of the input pulse to

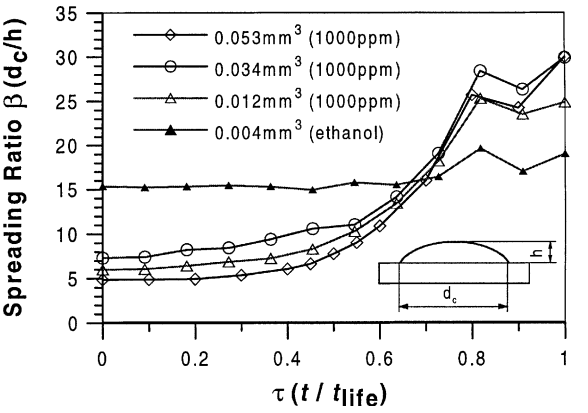

Fig. 12. Spreading ratio evolution of surfactant solution droplets (1000 ppm by weight) with different initial volumes ($T = 100$ °C).

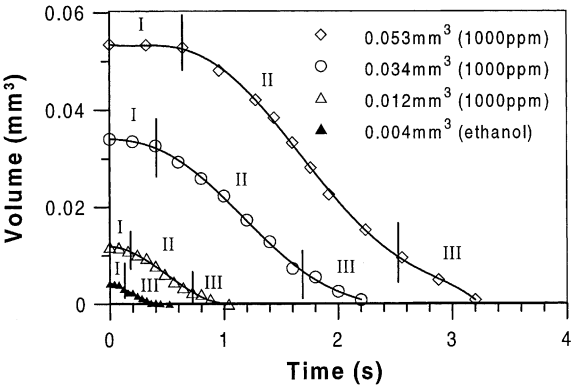

Fig. 13. Volume evolution of surfactant solution droplets (1000 ppm by weight) with different initial volumes ($T = 100$ °C).

the electromagnet shaker. The results are shown in Fig. 13. The evaporation curves for different volumes of same composition show similar trends.

5. Conclusion

A novel optical method to measure the contact diameter, profile, and volume of a liquid droplet evaporating on a hot solid substrate was developed. With the geometrical optics approach, the contact diameter and droplet profile can be derived from its scattering pattern. The contact diameter is related to the total number of scattering fringes and the profile is related to the spatial frequency. By assuming the droplet is axis symmetric, volume can be derived from the profile. The minimum measurable volume is 2.48×10^{-5} mm^3, which equals to the volume of a sphere with a diameter of 36 μm. An accuracy of ±1% for the contact diameter measurement

and ±5% for the volume measurement has been achieved. Further improvement in resolution is possible by using short wavelength lasers or smaller fringe spacing. The behaviors of evaporating ethanol and water microdroplets were investigated. Based on experimental data, it was found that the evaporation process could be divided into three regions namely, constant volume heating up, constant contact diameter evaporation, and constant contact angle evaporation. The reduction of contact angle during evaporation may be contributed by both the dynamics of rapid evaporation and the concentration variation of surfactant. This provides useful information in modeling the dropwise evaporation process.

References

[1] L.H.J. Wachters, N.A.J. Westerling, The heat transfer from a hot wall to impinging water drops in a spheroidal state, Chem. Eng. Sci. 21 (1966) 1047–1056.
[2] S. Toda, A study of mist cooling (1st Report: investigation of mist cooling), Heat Transfer Jap. Res. 1 (3) (1972) 39–50.
[3] S. Chandra, C.T. Avedisian, On the collision of a droplet with a solid surface, Proc. Royal Soc. London A 432 (1991) 13–41.
[4] T.Y. Xoing, M.C. Yuen, Evaporation of a liquid droplet on a hot plate, Int. J. Heat Mass Transfer 34 (7) (1991) 1881–1894.
[5] Y.M. Qiao, S. Chandra, Experiments on adding a surfactant to water drops boiling on a hot surface, Proc. Royal Soc. London A 453 (1997) 673–689.
[6] K.S. Haroon, L.E. Scriven, Measurement of liquid film profiles by Moiré topography, Chem. Eng. Sci. 38 (4) (1983) 525–534.
[7] C. Chan, N. Liang, W. Liu, Measurement of the shape of liquid–liquid interface by the method of light reflection, Rev. Sci. Instrum. 64 (1993) 632–637.
[8] T. Ohyama, K. Endoh, A. Mikami, Y. Mori, Optical interferometry for measuring instantaneous thickness of transparent solid and liquid films, Rev. Sci. Instrum. 59 (1988) 2018–2022.
[9] Y. Xu, N. Zhang, W.J. Yang, C.M. Vest, Optical measurement of profile and contact angle of liquids on transparent substrates, Exp. Fluids 2 (1984) 142–144.
[10] K.H. Guo, T. Uemura, W.J. Yang, Reflection-interference method to determine droplet profiles, Appl. Opt. 24 (16) (1985) 2655–2659.
[11] L. Thomas, R. Gratton, B. Marino, J. Diez, Droplet profiles obtained from the intensity distribution of refraction patterns, Appl. Opt. 34 (25) (1995) 5840–5847.
[12] W. Jia, H.-H. Qiu, A novel optical method in micro drop deformation measurements, Opt. Laser Eng. 35 (2001) 187–198.
[13] W. Jia, Study of spray cooling by advanced optical diagnostics, Ph.D. thesis, The Hong Kong University of Science and Technology, Hong Kong, June 2001.
[14] W.J. O'Brien, Capillary penetration of liquids between dissimilar solids, Ph.D. thesis, University of Michigan, Ann Arbor, Univ. Microfilm no. 6715666, 1967.
[15] S.S. Sadhal, M.S. Plesset, Effect of solid properties and contact angle in dropwise condensation and evaporation, J. Heat Transfer 101 (1979) 48–54.
[16] K.K. Tio, S.S. Sadhal, Dropwise evaporation: thermal analysis of multidrop systems, Int. J. Heat Mass Transfer 35 (8) (1992) 1987–2004.